Supporting Information (Manuscript ID NJ-ART-10-2011-020904)

Table S1. Details of hydrogen bonding parameters with symmetry code for **1-3**.

D-H...A	d(H...A) (Å)	d(D...A) (Å)	<D-H…A (°)
Compound 1			
N(1)-H(1C)...O(3) [1]	2.33	3.135(4)	164
O(3)-H(3)....O(4) [1]	1.89	2.677(4)	161
N(3)-H(3C)....O(6) [1]	2.15	2.908(4)	169
O(6)-H(6)....O(1) [1]	1.92	2.727(4)	169
O(9)-H(9D)....O(8) [1]	1.92(7)	2.844(6)	146(5)
O(9)-H(9C)....N(2) [2]	2.05(6)	2.913(5)	138(5)
C(28)-H(28B)….O(5) [3]	2.59	3.513(5)	159
C(45)-H(45A)....O(8) [4]	2.42	3.119(8)	129
C(45)-H(45B)....O(2) [1]	2.59	3.259(5)	126
C(55)-H(55)....O(2) [1]	2.28	2.864(5)	120
C(56)-H(56A) ….O(9) [5]	2.38	3.289(5)	157
C(62)-H(62) ..O(7) [6]	2.52	3.320(6)	145
C(71)-H(71B) ..O(7) [7]	2.49	3.408(7)	161
C(72)-H(72) ..O(2) [4]	2.42	3.165(7)	137

[1] x, y, z; [2] x, 3/2-y, 1/2+z; [3] 1/2-x, y, 1/2+z; [4] 1/2-x, 3/2-y, z; [5] x, 3/2-y, -1/2+z; [6] 1/2+x, 2-y ,1/2-z; [7] -x, -1/2+y, 1/2-z

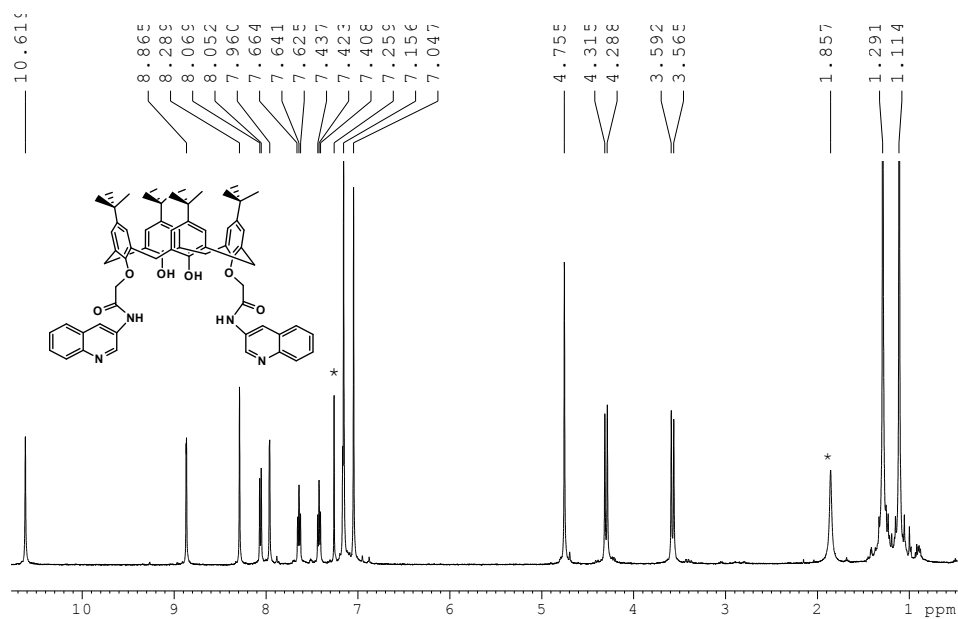|			
Compound 2			
N(1)-H(1C)....O(2) [1]	2.28(4)	3.067(5)	167(4)
O(2)-H(2)….O(3) [1]	1.94	2.744(4)	166
N(3)-H(3C)....O(4) [1]	2.40(4)	3.152(5)	172(3)
O(4)-H(4)....O(1) [1]	1.92	2.726(4	168
C(51)-H(51)....O(6) [2]	2.10	3.019(7)	156
[1] x, y, z; [2] 1+x,y,z;			
Compound 3			
N(1)-H(1C)…..N(4) [1]	2.02	2.959(3)	174
N(5) --H(5C)…..N(8) [1]	2.09	2.924(4)	172
C(110)--H(10E)…..O(5) [2]	2.35	3.2246(7)	150
C(11) --H(11) …..O(2) [3]	2.56	3.474(4)	167
C(112)--H(12F)…..O(5) [2]	2.54	3.384(5)	148
C(53) --H(53)…..O(1) [1]	2.47	3.359(2)	160
C(88) --H(88)…..O(8) [1]	2.32	2.900(3)	120
C(109)--H(109)…..O(7) [1]	2.43	3.214(6)	142
[1] x, y, z;			

Fig. S1. ^{1}H NMR spectrum of the compound **1** recorded in CDCl$_3$, signals with

* mark is from solvent.

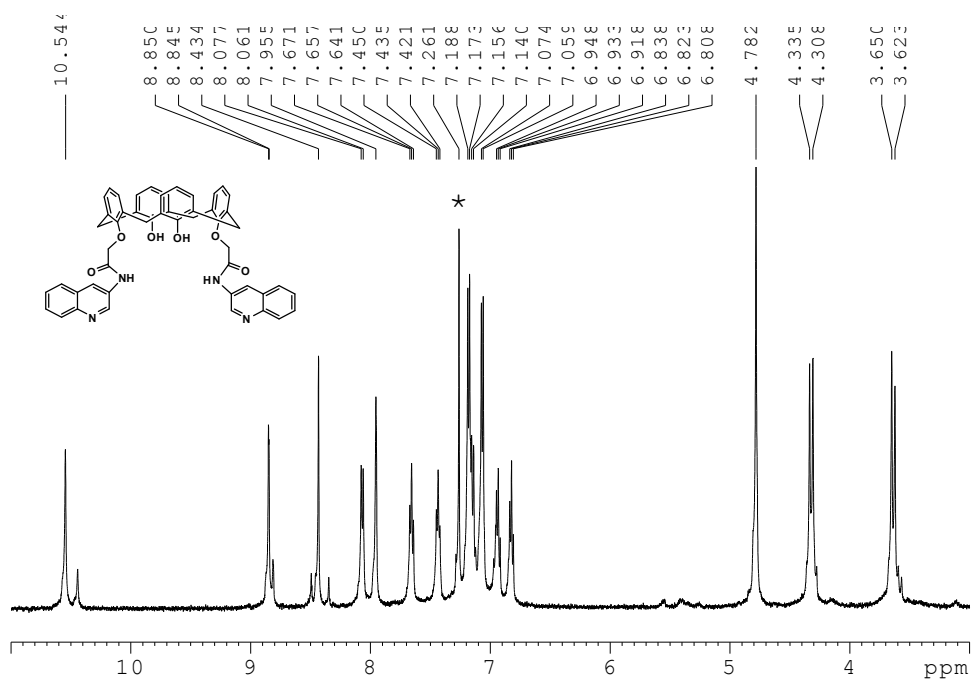Fig. S2. ^{1}H NMR spectrum of the compound **2** recorded in CDCl$_3$, signal with * mark is from solvent.
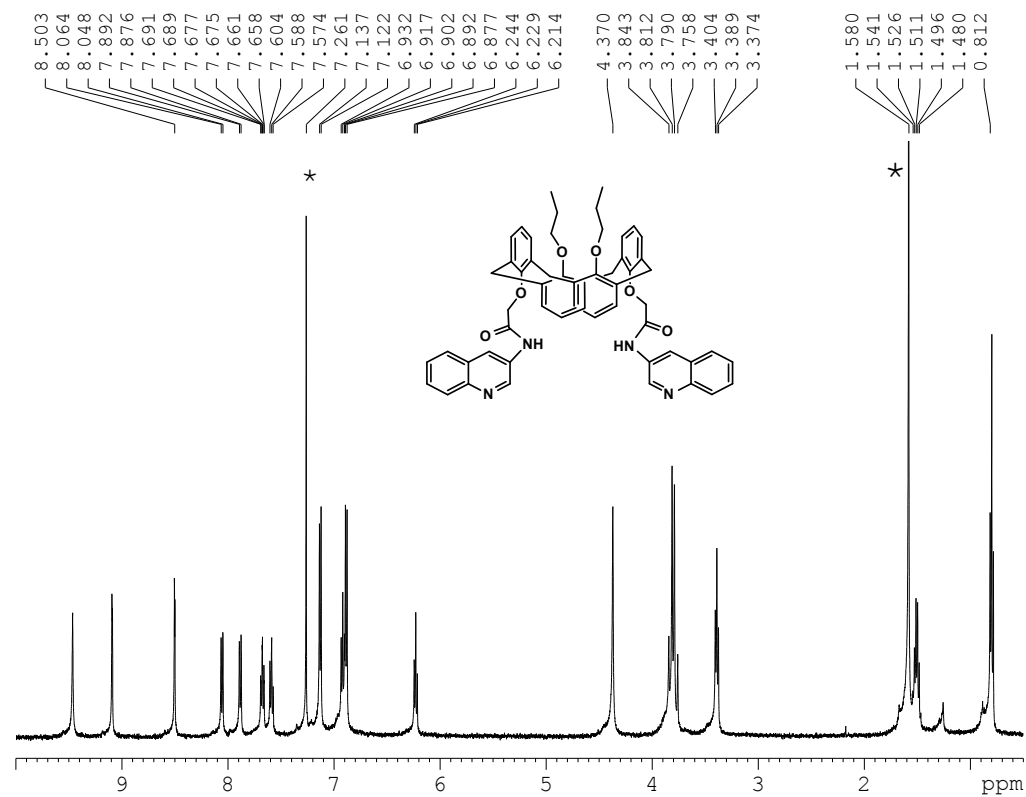
Fig. S3. ^{1}H NMR spectrum of the compound **3** recorded in CDCl$_3$, signals with *
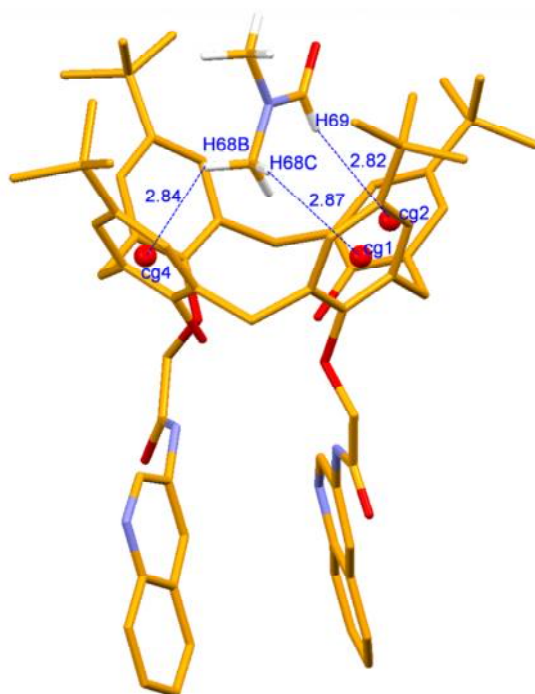
mark are from solvent.

Fig. S4. Mercury diagram of **1** depicting the encapsulation of DMF molecule inside the calix cone making C-H…π interactions.

Details of interaction: The methyl hydrogens H68B and H68C of the DMF molecule is involved in C-H….π interaction with H….Cg (centroid of the benzene ring), distance 2.84 and 2.87 Å respectively. The amide hydrogen H69 is also involved in C-H….π interaction with H….Cg distance of 2.82 Å with another benzene ring of the calix. Details parameters for the interactions are: C(68)-H(68B)….Cg(4): H(68B)…..Cg(4) = 2.84; C(68)…..Cg(4) = 3.445(5); <C(68)-H(68B)…..Cg(4) = 122: symmetry code; x,y,z; C(68)-H(68C)…..Cg(1): H(68C)…..Cg(1) = 2.87; C(68)…..Cg(1) = 3.536(5); <C(68)-H(68C)…..Cg(1) = 127: symmetry code; x,y,z; C(69)-H(69)…..Cg(2): H(69)…..Cg(2) = 2.82; C(69)…..Cg(2) = 3.725(5); <C(69)-H(69)…. Cg(2) = 164: symmetry code: x,y,z; where Cg(1), Cg(2) and Cg(4) are centroids of the phenyl rings C1-C6, C8-C13 and C22-C27, respectively.
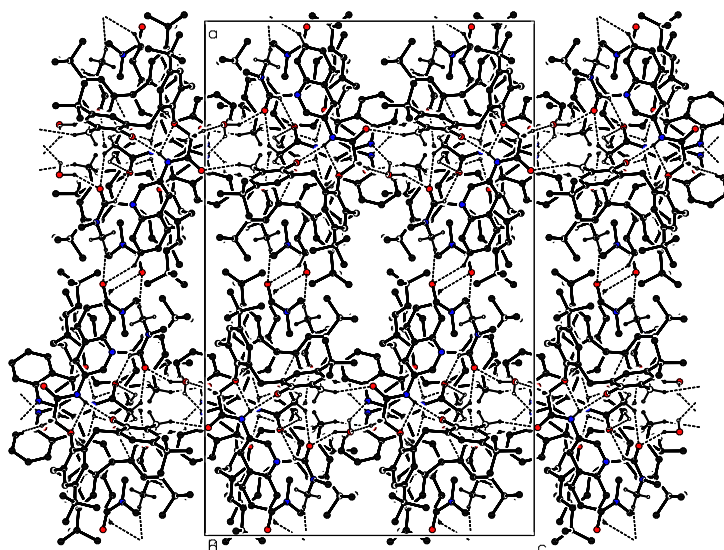
Fig. S5. Packing diagram of compound **1** with hydrogen bonding interaction viewed down c-axis depicting the two dimensional H-bonding network along ab-plane.
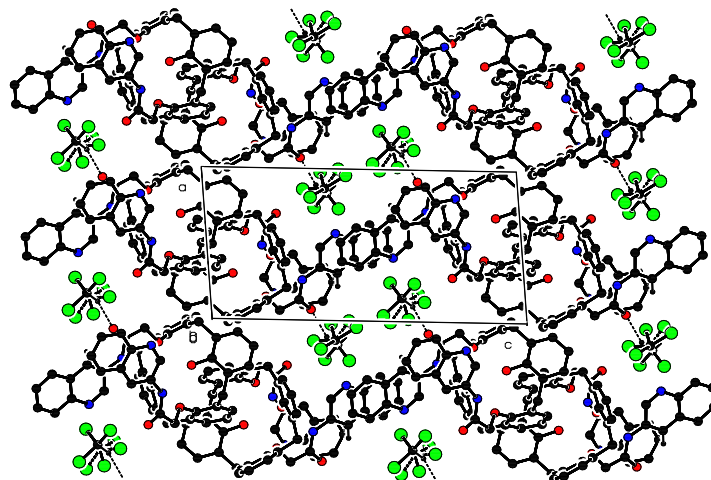
Fig. S6. Packing diagram of **2** viewed down b-axis depicting the Zigzag orientation of the calix moiety with the orientation of the chloroform molecule between the adjacent zigzag layers.
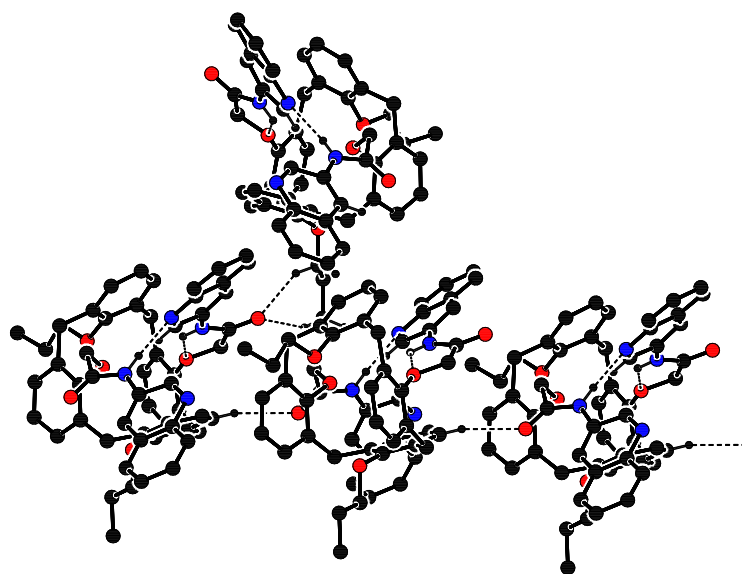
Fig. S7. Close-up view depicting the C-H….O hydrogen bonding interaction between both the molecules of **3** present in the asymmetric unit in the formation of zigzag layers.
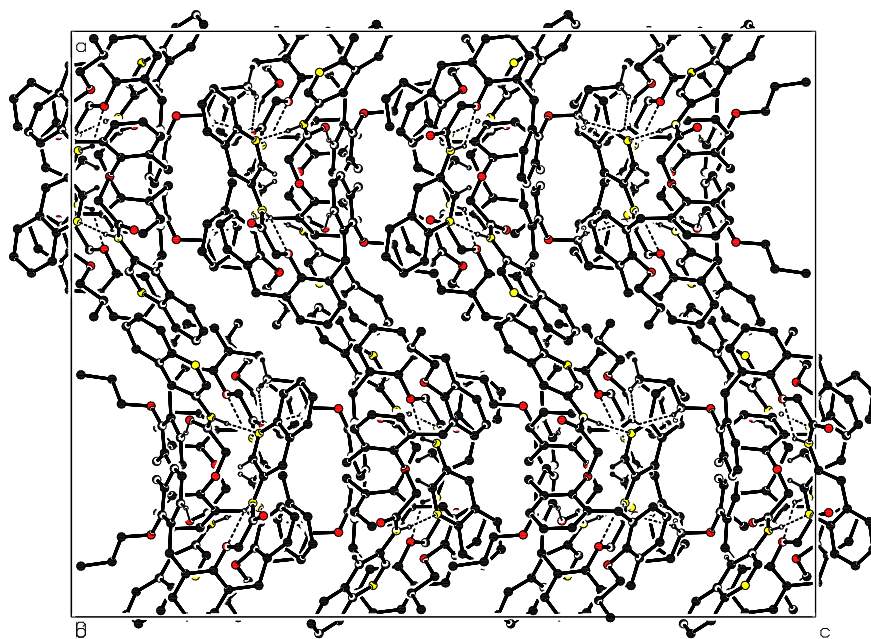
Fig. S8. Packing diagram with hydrogen bonding interaction for compound **3** viewed down b-axis showing the zigzag arrangement of the calix moiety in layers linked via hydrogen bonding and π stacking interactions.
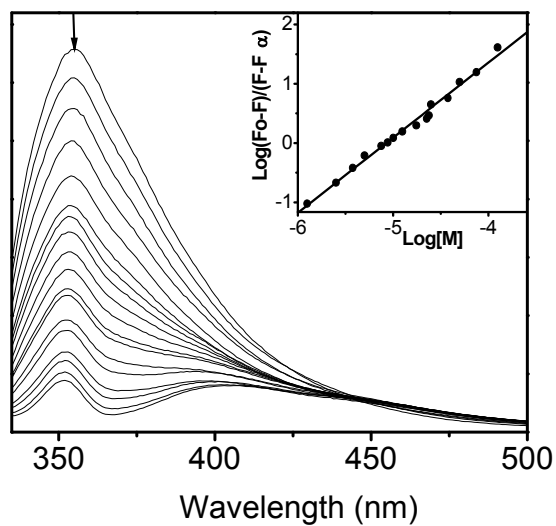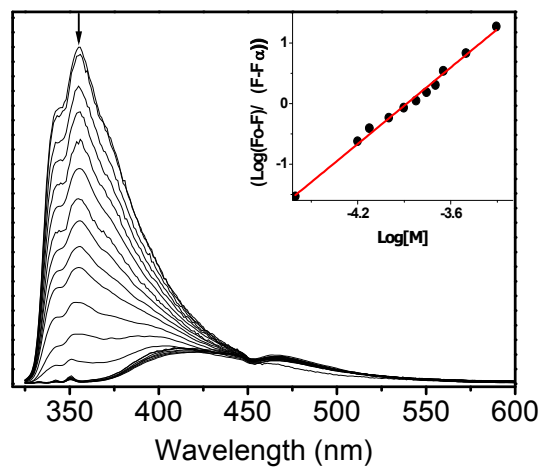
Fig. S9. Emission spectral changes for **2** (2.5×10^{-6} M) upon addition of increasing concentration of Pb(ClO$_4$)$_2$. Excitation wavelength: 318 nm. Inset: linear regression fit (double-logarithmic plot) of the titration data as a function of concentration of metal ion.
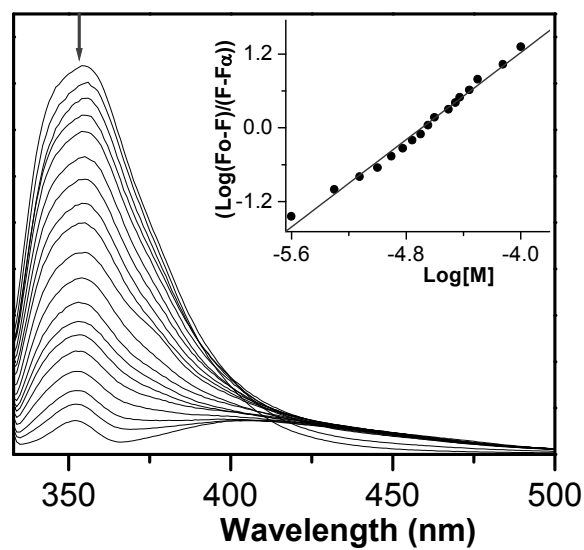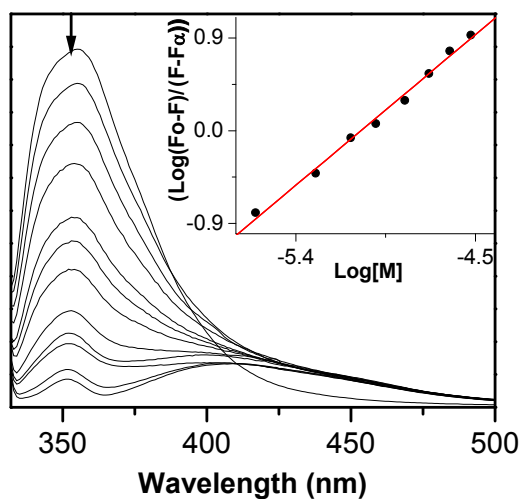
Fig. S10. Emission spectral changes for **2** (2.5×10^{-6} M) upon addition of increasing concentration of $Fe(ClO_4)_2$. Excitation wavelength: 318 nm. Inset: linear regression fit (double-logarithmic plot) of the titration data as a function of concentration of metal ion.
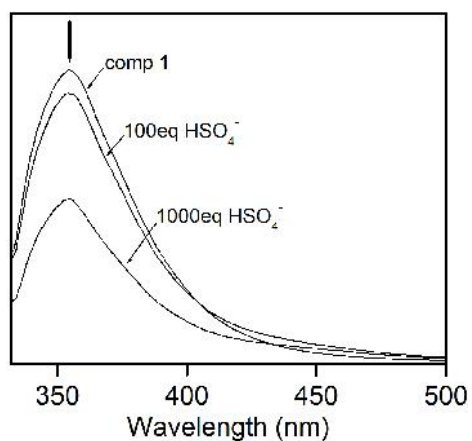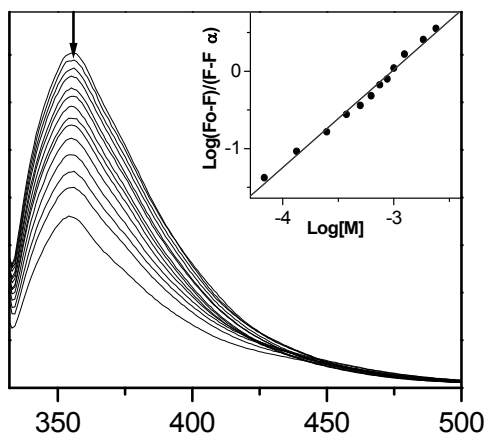
Fig. S11. Emission spectral changes for **3** (2.5×10^{-6} M) upon addition of increasing concentration of $Pb(ClO_4)_2$. Excitation wavelength: 321 nm. Inset: linear regression fit (double-logarithmic plot) of the titration data as a function of concentration of metal ion.

Fig. S12. Emission spectral changes for **3** (2.5×10^{-6} M) upon addition of increasing concentration of $Fe(ClO_4)_3$. Excitation wavelength: 321 nm. Inset: linear regression fit (double-logarithmic plot) of the titration data as a function of concentration of metal ion.

(a)

(b)

Fig. S13.   Emission spectral changes for **1** (a) and **2** (b) (2.5×10^{-6} M) upon addition of increasing concentration of HSO_4^-. Excitation wavelength: 318 nm. Inset for (a): linear regression fit (double-logarithmic plot) of the titration data as a function of concentration of metal ion.
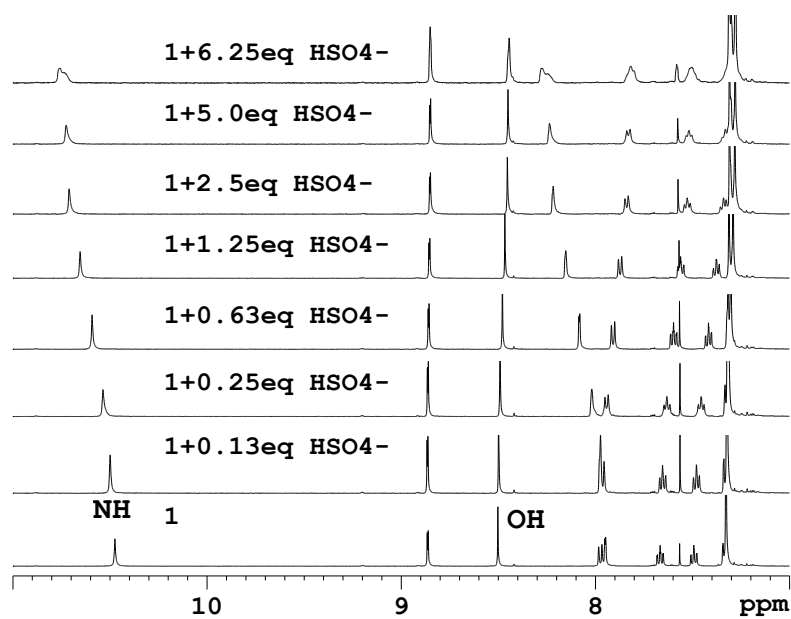
Fig. S14. Selected portion of the ^{1}H NMR spectral change for **1** upon addition of the increasing amount of HSO_4^-
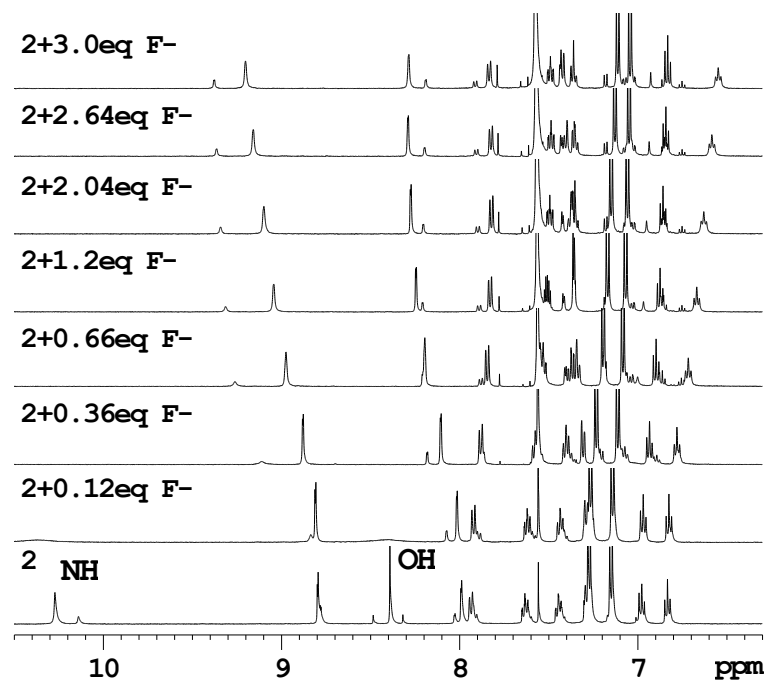
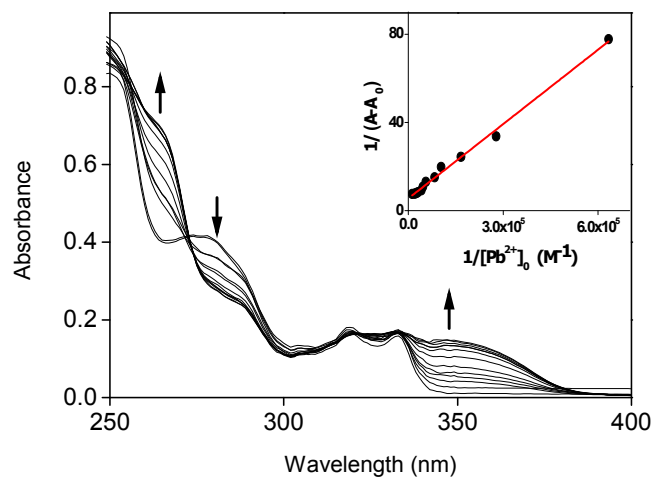Fig. S15. Selected portion of the ^{1}H NMR spectral change for **2** upon addition of the increasing amount of F$^-$

Fig. S16. Uv-vis spectral changes for **1** (2.5×10^{-5} M) upon addition of increasing amount of Pb(ClO$_4$)$_2$ in acetonitrile.
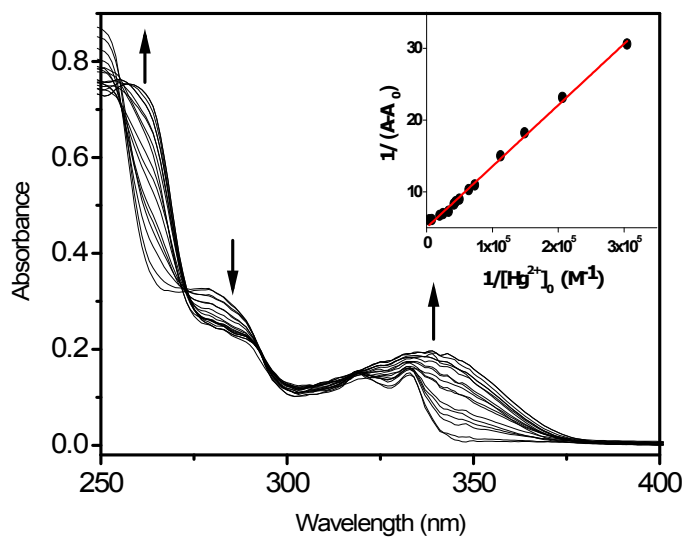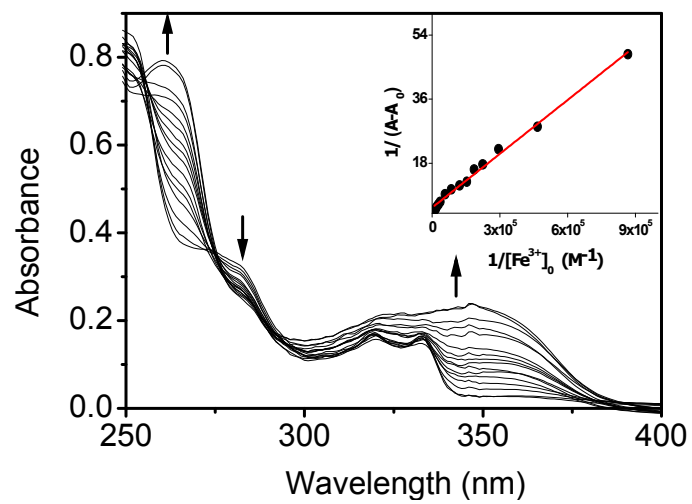
Fig. S17. Uv-vis spectral change for **1** (2.5×10^{-5} M) upon addition of increasing amount of Hg(ClO$_4$)$_2$ in acetonitrile.

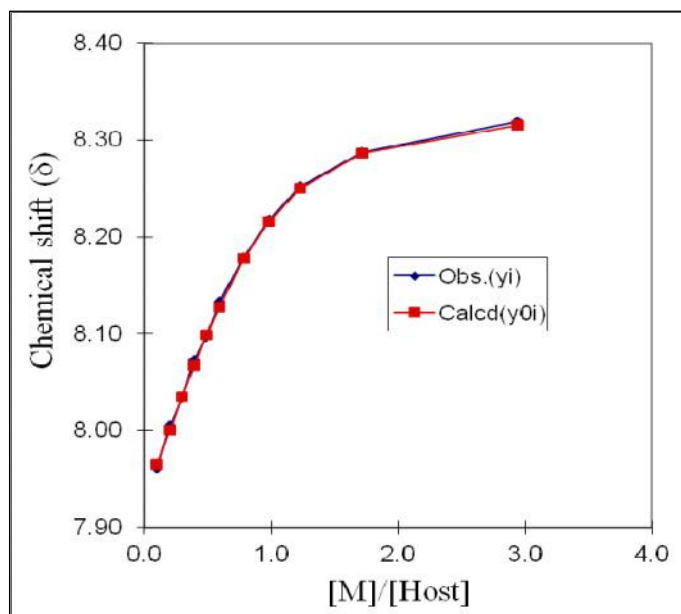Fig. S18. Uv-vis spectral change for **1** (2.5×10^{-5} M) upon addition of increasing amount of Fe(ClO$_4$)$_3$ in acetonitrile.

Fig. S19. The non-linear least square fit from ^{1}H NMR titration data for the determination of binding constant for **1** with F[-] in CD_3CN-$CDCl_3$ (4:1).
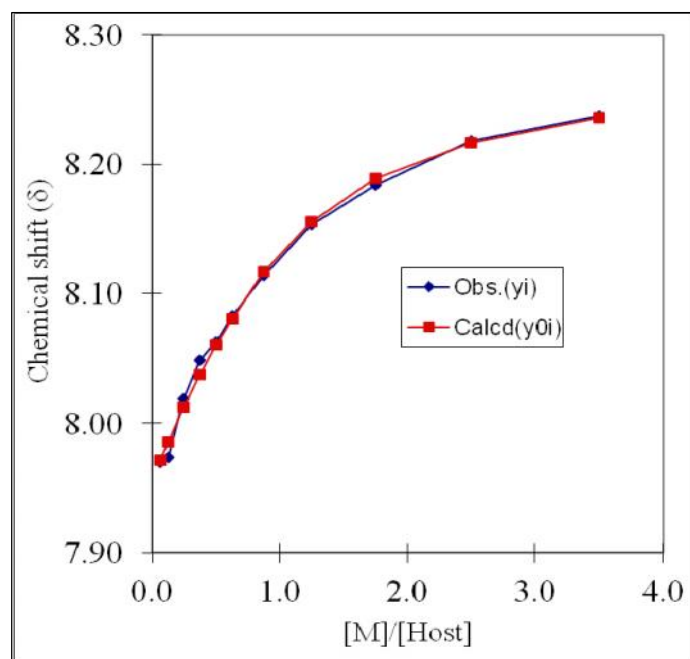
Fig. S20. The non-linear least square fit from ^{1}H NMR titration data for the determination of binding constant for HSO_4^- with F^- in CD_3CN-$CDCl_3$ (4:1).
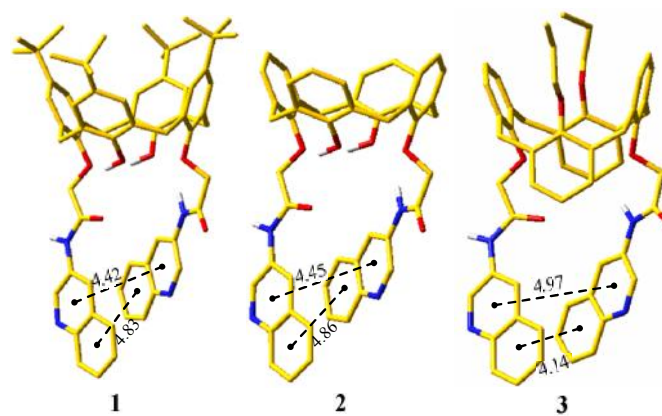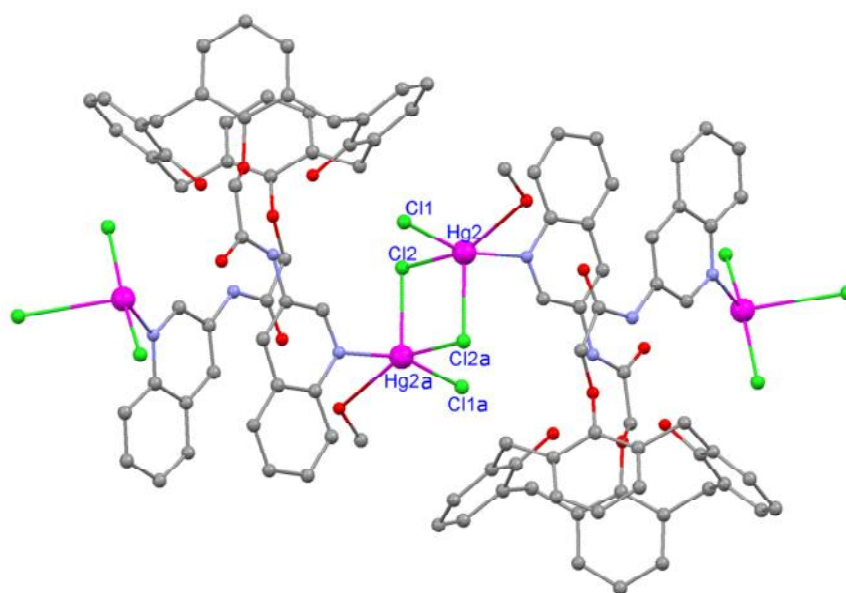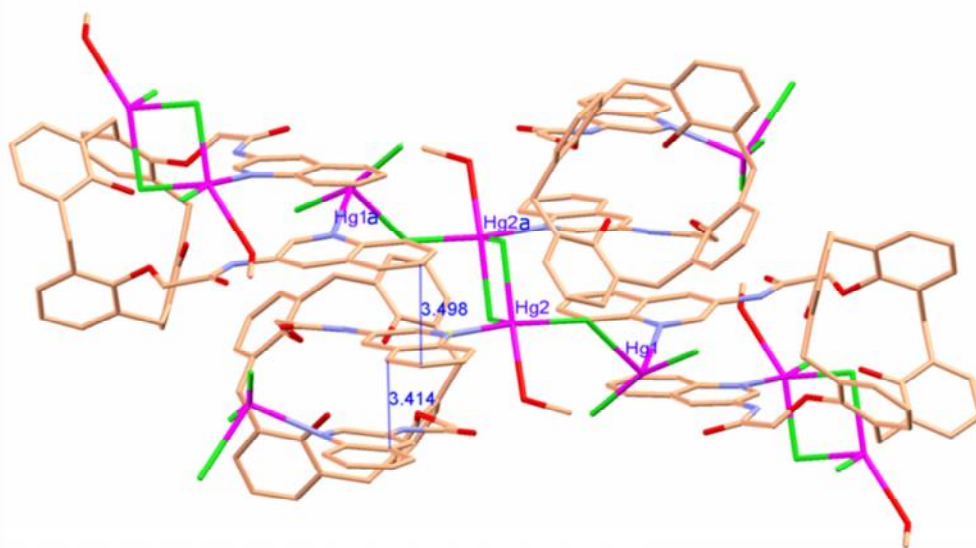
Fig. S21. Calculated lowest energy conformations of compound **1**-**3** in molecular mechanics (MMFF94) force field using Monte Carlo search method in acetonitrile solvent (distances are in Å) (yellow = carbon, red = oxygen; blue = nitrogen; white = hydrogen).
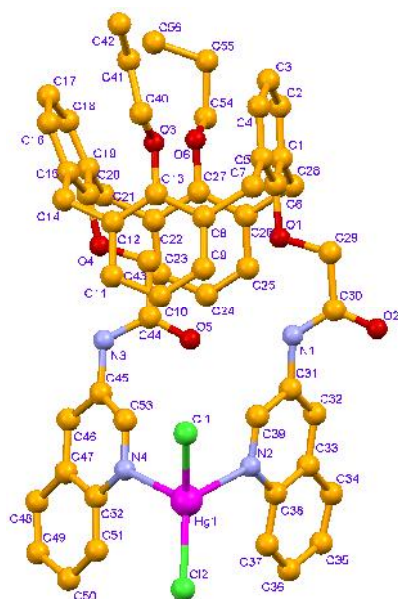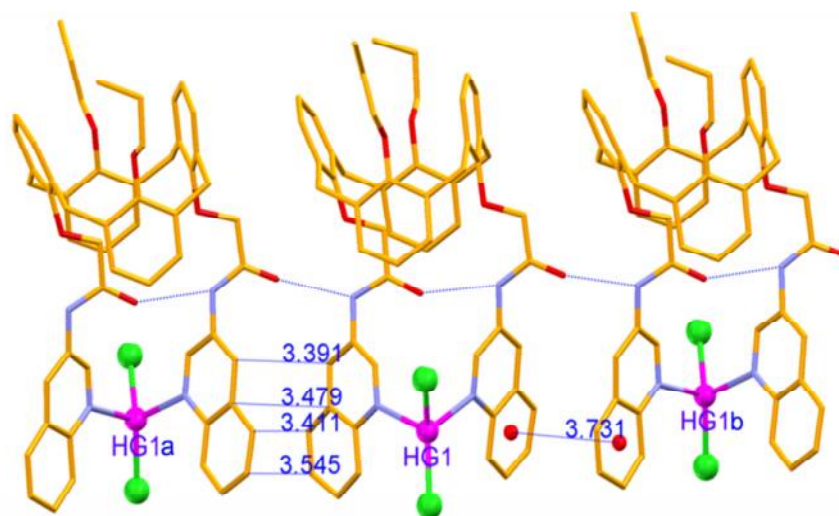
(a)

(b)

Fig. S22. (a) Crystal structure of the Hg^{2+} complex of **2** showing coordination pattern of Hg^{2+} (hydrogen atoms are omitted for clarity) and (b) intermolecular π....π stacking interactions involving quinoline moieties. (symmetry transformation used to generate equivalent atoms :1-x, -y -z)

(a)

(b)

Fig. S23. (a) Crystal structure of the Hg^{2+} complex of **3** with atom numbering scheme (hydrogen atoms and lattice solvent molecules are omitted for clarity); (b) intermolecular N-H...O hydrogen bonding and π....π stacking interactions involving quinoline moieties. symmetry transformation used to generate equivalent atoms a: x, 1/2-y , 1/2–z   b: x, 1/2-y , ½+z)
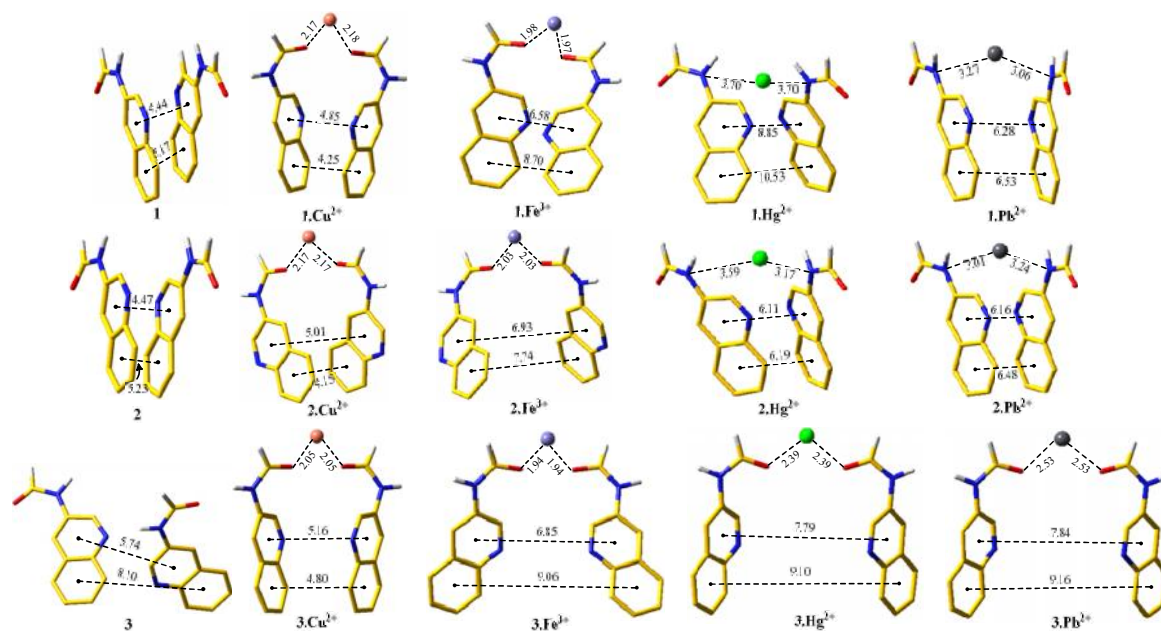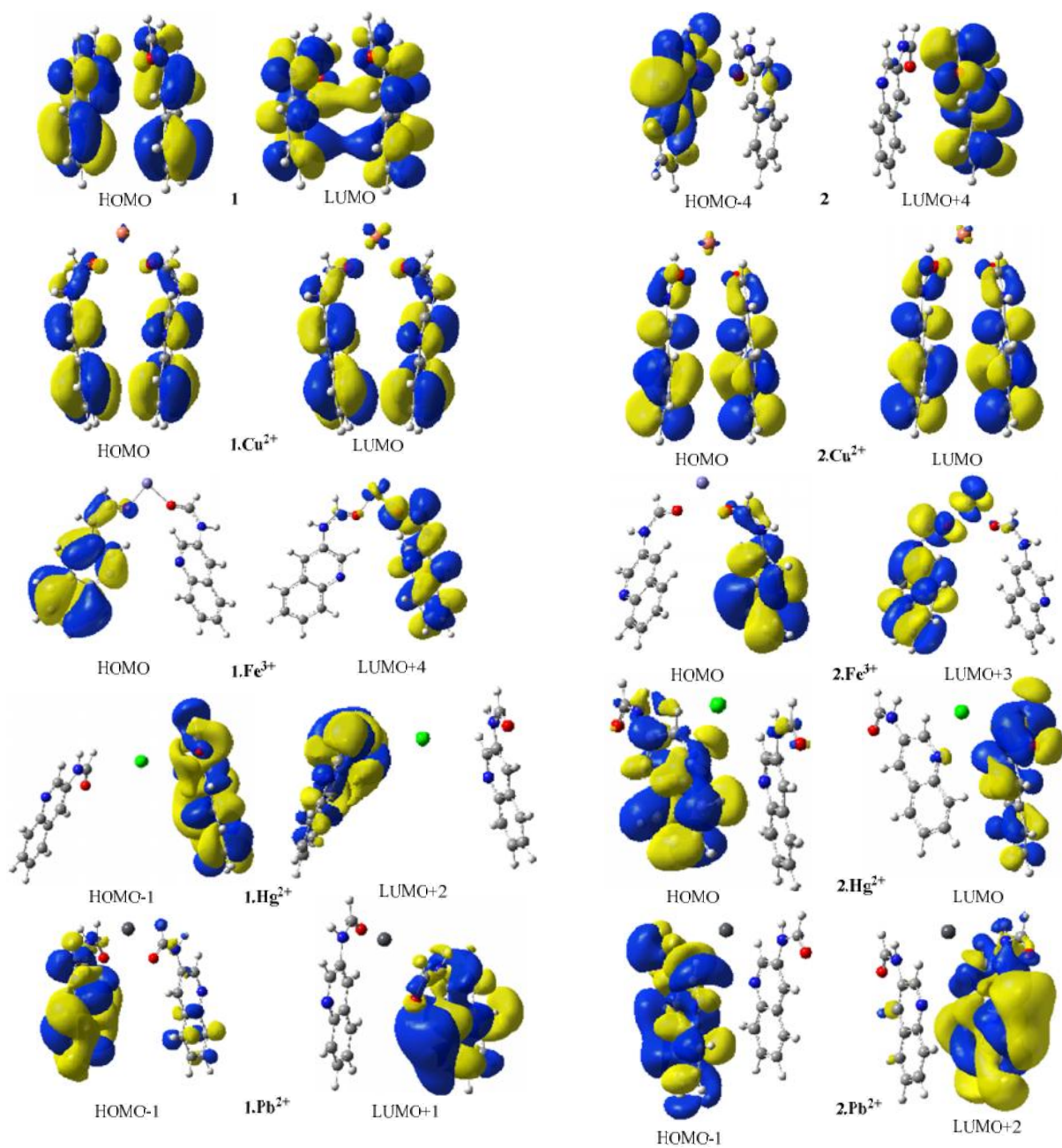
Fig. S24. GGA/PW91/DND calculated model geometries of ionophores **1-3** and its metal ion complexes for frontier molecular orbital analysis at M05-2X/6-31G* level (distances are in Å) (yellow = carbon, red = oxygen; blue = nitrogen; white = hydrogen).

HOMO   **1**   LUMO   HOMO-4   **2**   LUMO+4

HOMO   **1.Cu^{2+}**   LUMO   HOMO   **2.Cu^{2+}**   LUMO

HOMO   **1.Fe^{3+}**   LUMO+4   HOMO   **2.Fe^{3+}**   LUMO+3

HOMO-1   **1.Hg^{2+}**   LUMO+2   **2.Hg^{2+}**   HOMO   LUMO

HOMO-1   **1.Pb^{2+}**   LUMO+1   **2.Pb^{2+}**   LUMO+2   HOMO-1
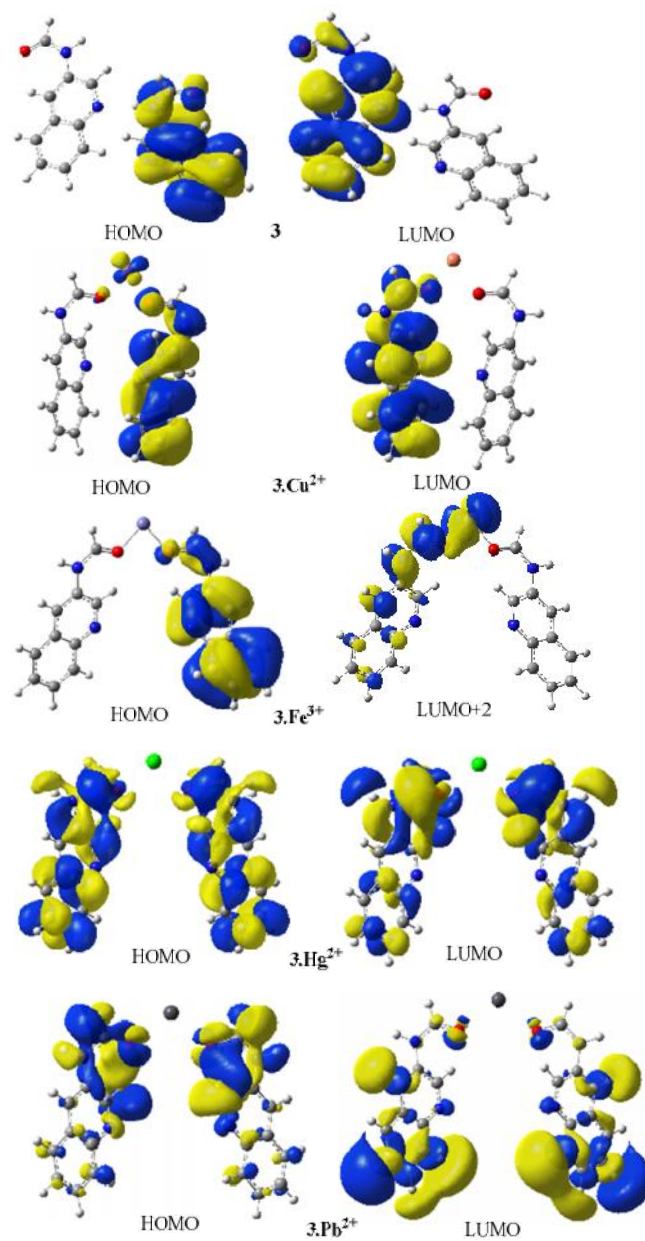
Fig. S25. GGA/PW91/DND calculated model geometries of ionophores **1-3** and its metal ion complexes used to derive frontier molecular orbitals at M05-2X/6-31G* level.
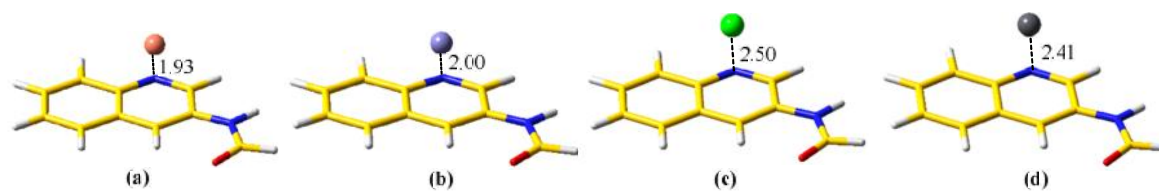
Fig. S26. Optimized geometries of quinoline rings with (a) Cu^{2+}, (b) Fe^{3+}, (c) Hg^{2+}, (d) Pb^{2+} at GGA/PW91/DND level (distances are in Å) (yellow = carbon, red = oxygen; blue = nitrogen; white = hydrogen).
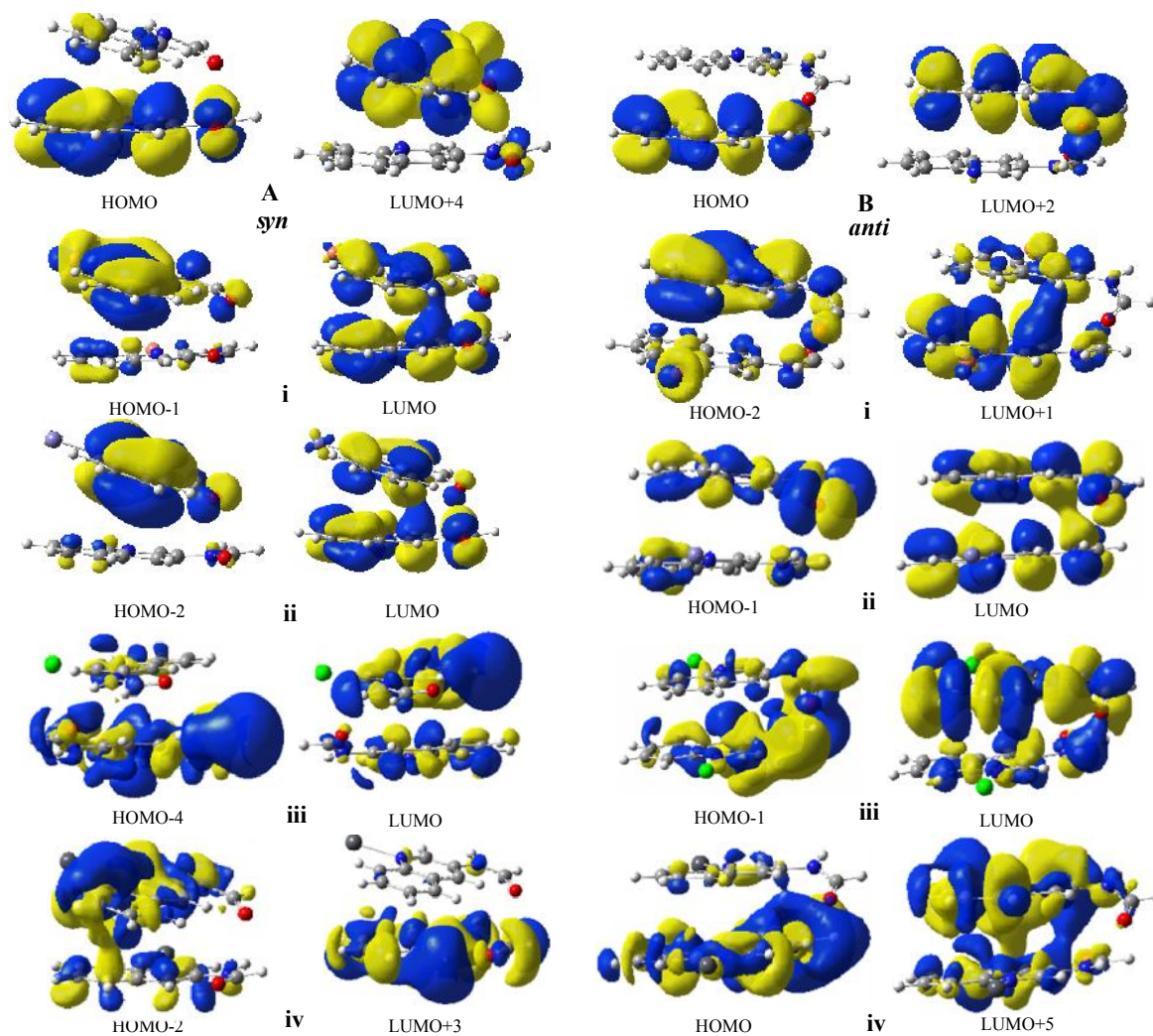
Fig. S27. Frontier molecular orbitals of modeled quinoline moieties and its metal ion complexes in *syn* (A) and *anti* (B) arrangements at M05-2X/6-31G* level.
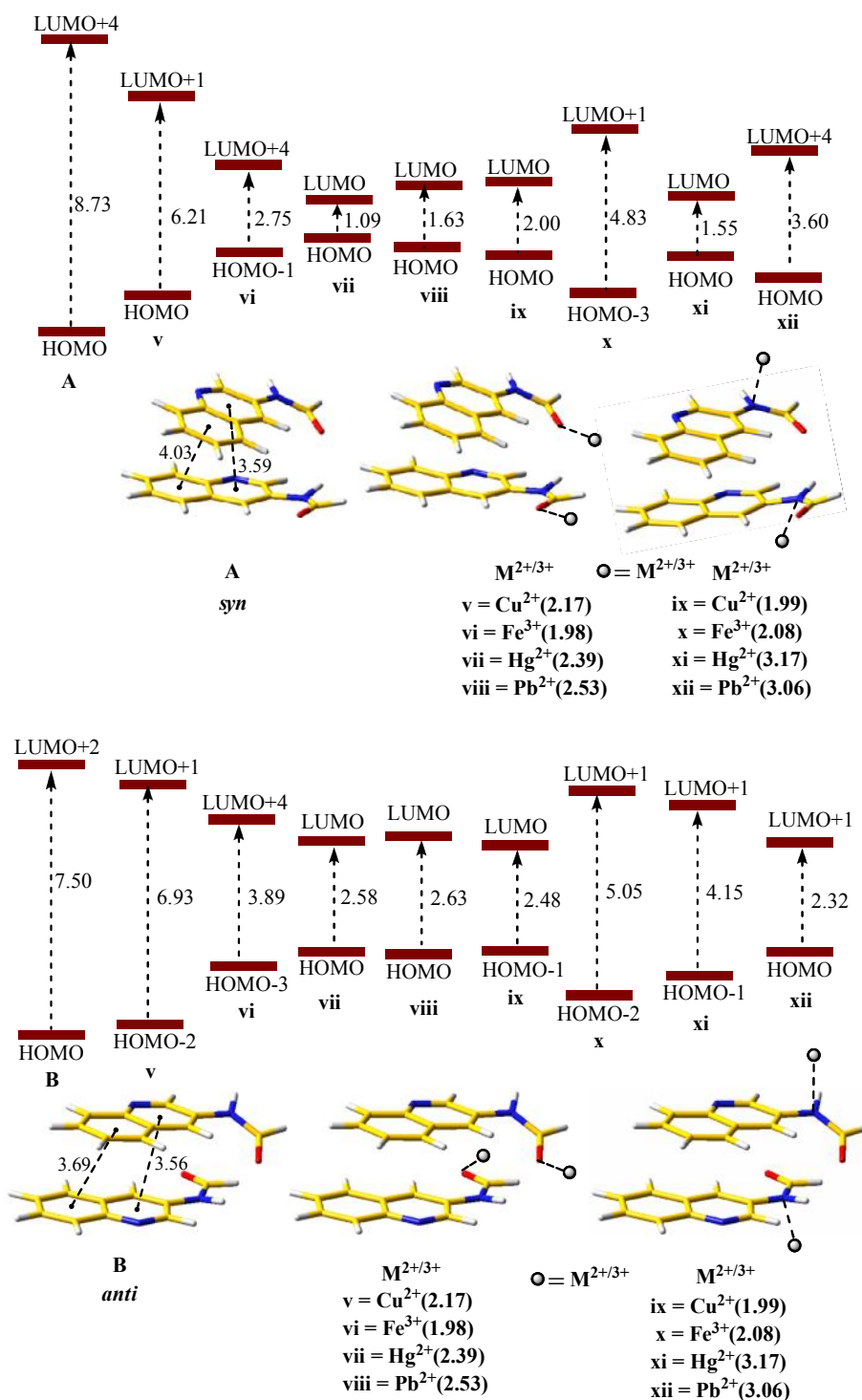
Fig. S28. Frontier molecular orbital energy levels of modeled quinoline moieties and its metal ion complexes in *syn* (A) and *anti* (B) arrangements at M05-2X/6-31G* level (energies are in eV and distances in Å) (yellow = carbon, red = oxygen; blue = nitrogen; white = hydrogen).
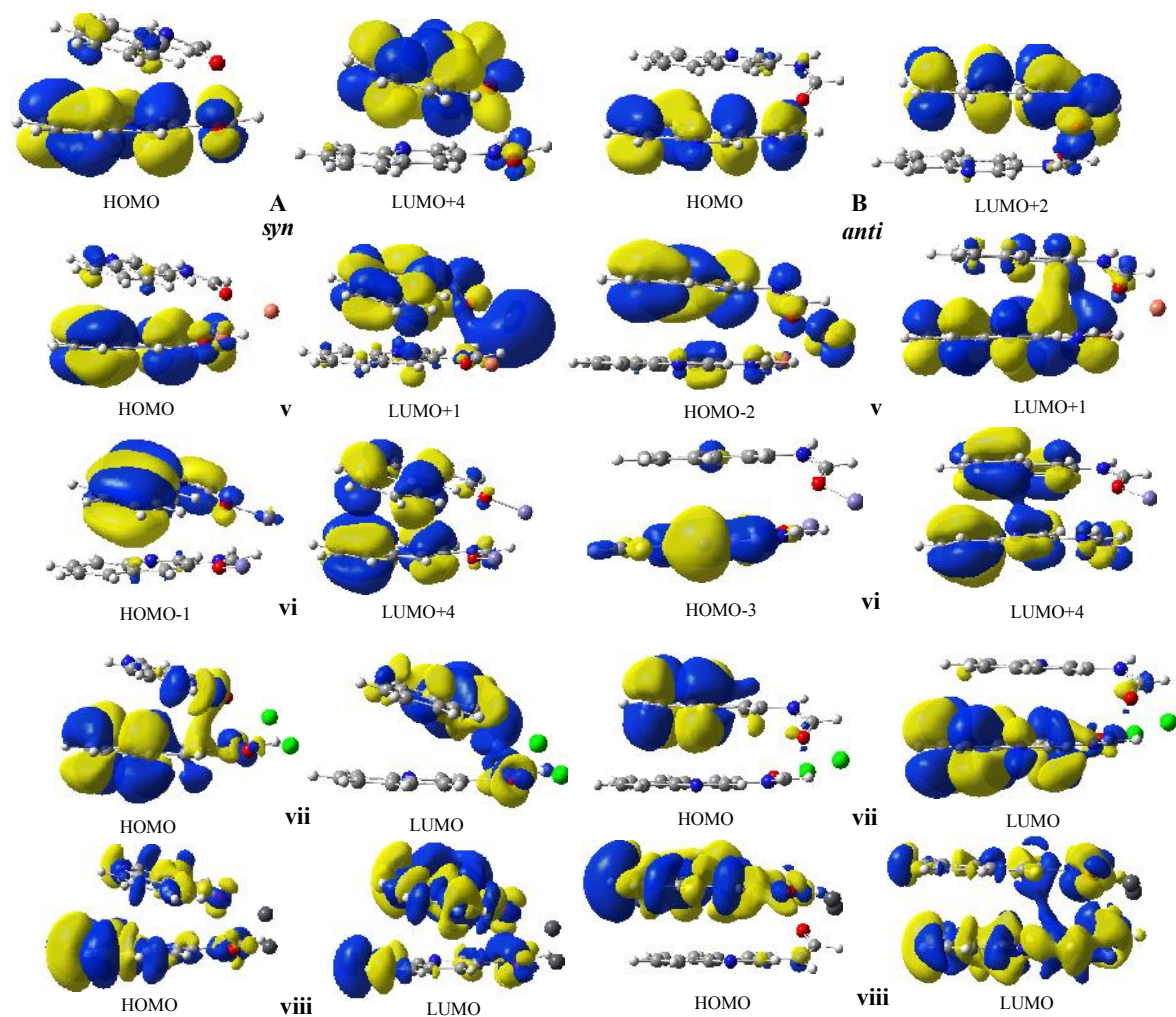
Fig. S29. Frontier molecular orbitals of modeled quinoline moieties and its metal ion complexes with amide oxygen atom in *syn* (A) and *anti* (B) arrangements at M05-2X/6-31G* level.
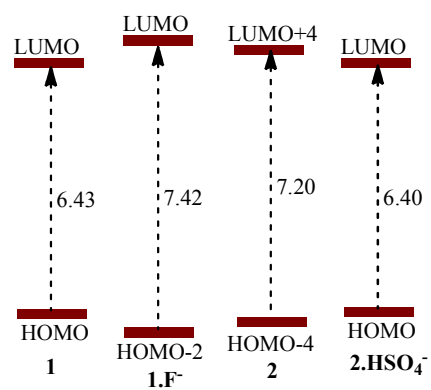
Fig. S30. Frontier molecular orbital energy levels of modeled ionophores **1** and **2** with F$^-$ and HSO$_4^-$ respectively at M05-2X/6-31G* level (energies are in eV).

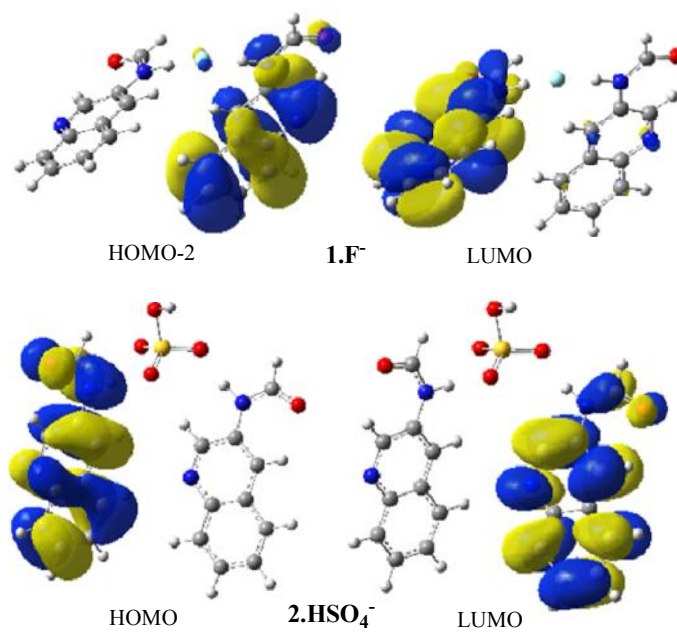HOMO-2   **1.F⁻**   LUMO

HOMO   **2.HSO₄⁻**   LUMO

Fig. S31. GGA/PW91/DND calculated model geometries of anion complexes 1.F⁻ and 2.HSO₄⁻ used to derive frontier molecular orbitals at M05-2X/6-31G* level.